Title

Brain-Mimetic 3D Culture Platforms Allow Investigation of Cooperative Effects of Extracellular Matrix Features on Therapeutic Resistance in Glioblastoma

Journal

Cancer Research, 78(5)

ISSN

0008-5472

Authors

Xiao, Weikun
Zhang, Rongyu
Sohrabi, Alireza
et al.

Publication Date

2018-03-01

DOI

10.1158/0008-5472.can-17-2429

Peer reviewed

Brain-Mimetic 3D Culture Platforms for Investigating Cooperative Effects of Extracellular Matrix Features on Therapeutic Resistance in Glioblastoma

Weikun Xiao[1], Rongyu Zhang[1], Alireza Sohrabi[1], Arshia Ehsanipour[1], Songping Sun[1], Jesse Liang[1], Christopher Walthers[1], Lisa Ta[2], David A. Nathanson[2,3,4], and Stephanie K. Seidlits[1,3,4,5]

[1]Department of Bioengineering, University of California, Los Angeles, CA, 90095
[2]Department of Molecular and Medical Pharmacology, University of California, Los Angeles, CA, 90095
[3]Jonsson Comprehensive Cancer Center, University of California, Los Angeles, CA, 90095
[4]Brain Research Institute, University of California, Los Angeles, CA, 90095
[5]Broad Stem Cell Research Center, University of California, Los Angeles, CA, 90095

Running title: Glioblastoma Drug Resistance in 3D Cultures

Keywords: Glioblastoma, Biomimetic Platform, Drug resistance, Matrix Hyaluronan, Biomaterial

Corresponding author:

Stephanie K. Seidlits, Ph.D.
Assistant Professor, Bioengineering
University of California Los Angeles
420 Westwood Plaza, Engineering V, room 5121H
Los Angeles, CA 90095
Phone: 310-267-5244
Email: seidlits@g.ucla.edu

Conflict of Interest: The authors declare no potential conflicts of interest.

Word count in text (abstract to end of discussion): 5265

Total number of Figures: 7

Total number of tables:0

Financial support: This work was supported with funding from the NIH (R21NS093199) and the UCLA ARC 3R's Award.

Abstract

Glioblastoma (GBM) is a highly aggressive brain cancer with poor prognosis. GBM tumors exhibit potentially actionable genetic alterations against which targeted therapies have proven successful in treatment of other cancers. However, the same treatments have largely failed in GBM patients. A notable example is pharmacological inhibition of epidermal growth factor receptor (EGFR), for which clinical efficacy has been poor despite overexpression and/or mutation of EGFR in over 50% of GBM tumors. The lack of clinical translation may be attributed to the fact that conventional preclinical models (e.g., cell culture and heterotypic xenografts) fail to account for interactions of GBM cells with the unique brain extracellular matrix (ECM) – enriched in hyaluronic acid (HA) and relatively soft – which may facilitate drug resistance. Here, we present a biomaterial platform providing a brain-mimetic, artificial ECM for 3D-cultured, patient-derived GBM cells as an experimental model with improved physiological accuracy. Compared to orthotopic xenografts, biomaterial cultures better preserved physiology and kinetics of acquired resistance to the EGFR inhibition than gliomasphere cultures. Orthogonal modulation of both HA content and mechanical properties of biomaterial scaffolds was required to achieve this result. Furthermore, interactions between GBM cell receptors and scaffold components significantly contributed to resistance to the cytotoxic effects of EGFR inhibition.

Introduction

Glioblastoma (GBM) is the most common and aggressive cancer originating in the central nervous system (CNS)(1). High lethality is largely attributed to poor therapeutic response to current treatments(2). Similar to many peripheral cancers, the epidermal growth factor receptor (EGFR), a receptor tyrosine kinase (RTK), is overexpressed and/or mutated in more than 50% of GBM tumors(2). EGFR stimulation activates the PI3K-AKT and MAPK-ERK pathways to promote progression, invasion, survival, and drug resistance(3). Targeted inhibition of EGFR have been largely successful in treatment of non-CNS malignancies with EGFR amplification and/or mutation, including breast cancer and non-small cell lung carcinoma(4,5). However, EGFR inhibition has been largely ineffective against GBM in clinical trials(6).

We contend that the unique brain microenvironment substantially contributes to the failure of targeted EGFR therapies in GBM. In contrast to malignant cancers of peripheral origin, GBM rarely metastasizes beyond the brain(7), indicating a strong preference for the brain microenvironment. The long chain polysaccharide hyaluronic acid (HA) is abundant in brain extracellular matrix (ECM), where it provides structural support. In GBM, overexpression of HA is associated with many phenotypic changes associated with cancer progression including initial tumor development, cancer cell proliferation, invasion, resistance to therapeutic agents and post-treatment recurrence(8). Likewise, cell surface receptors for HA, including CD44 and CD168 (i.e., HMMR or RHAMM), are often upregulated on GBM cells(9–11) and increased CD44 expression in clinical GBM tumors is a poor prognostic indicator(12).

Increased deposition of ECM proteins – which interact with integrins through the RGD sequence – directly correlates with poor GBM prognosis(13–16). Treatment of GBM with Cilengitide – a cyclic RGD peptide designed to inhibit RGD interactions with integrin $\alpha_v\beta_3$ – has shown modest success as an adjunct therapy to prevent integrin-mediated protection from drug-induced apoptosis in clinical trials(17). However, “inside-out” activation of integrin β_1 by HA-bound CD44 can bypass direct integrin-ECM interactions to promote survival of gastrointestinal, breast and ovarian cancer cells(18–20). Mechanical signaling from the GBM microenvironment, which is stiffer than normal brain, have also been reported to influence drug resistance(16,21). Integrins, CD44 and RTKs are mechanoresponsive(15,22–24).

Taken together, previous reports indicate that interactions among various ECM receptors act to protect cancer cells from drug-induced apoptosis and facilitate resistance. Thus, we posit that GBM tumors acquire resistance to EGFR inhibition through interactions with the local ECM, alternatively activating oncogenic pathways through both cooperation with and compensation for EGFR. However, the influence of the local microenvironment on therapeutic resistance in GBM has been challenging to study, as currently available experimental models fail to account for the complex array of ECM components surrounding GBM tumors and do not adequately reflect clinical outcomes. To address this limitation, we have developed a novel biomaterial platform

for three-dimensional (3D) culture of patient-derived GBM cells in which HA content, integrin-binding peptide concentration and compressive modulus can be orthogonally tuned to mimic GBM tumors.

Using this hydrogel platform, 3D-cultured GBM cells developed rapid resistance to erlotinib – a small molecule for targeted inhibition of EGFR currently used in clinical treatment of several cancers(4,5). Unlike patient-matched gliomasphere cultures, biomaterial-cultured GBM cells maintained expression of ECM receptors and resistance kinetics similar to orthotopic xenografts in mice. Orthogonal tuning of both HA content and scaffold compressive modulus was required to achieve these results – where a soft, HA-rich microenvironment that mimicked native brain was necessary to protect GBM from cytostatic and cytotoxic effects of erlotinib treatment. Furthermore, results demonstrate that these effects are at least partially mediated by HA-CD44 interactions. Finally, biomaterial cultures demonstrated the cooperative effects of integrin and CD44 engagement, where inclusion of RGD peptides into soft, HA-rich hydrogels significantly increased apoptotic resistance to erlotinib treatment. In future studies, these *ex vivo* culture platforms can provide 1) a controlled experimental space in which to quantify the independent and combined effects of individual ECM components on drug resistance and 2) more accurate predictions of *in vivo* tumor physiology.

Material and Methods

All reagents and materials were purchased from ThermoFisher Scientific (Waltham, MA USA), unless otherwise specified. More details on procedures can be found in supplementary methods.

Mouse xenografts: All studies were approved by the UCLA Office of Animal Rights Oversight. For intracranial experiments, GBM39 or HK301 cells with constitutive expression of gaussia luciferase were injected (2×10^5 cells) into the right striatum (2 mm lateral and 1 mm posterior to bregma, at a depth of 2 mm) of female nod-SCID-gamma mice (6-8 weeks old). Tumor burden was monitored semi-weekly via bioluminescence imaging using an IVIS 200 instrument. Two weeks following injection, mice were randomized into two treatment arms – vehicle or erlotinib. Mice were euthanized when moribund, which was defined by a loss of 25-30% body weight from start of treatment in addition to symptoms such as neurological defects, paralysis, hydrocephalus and hunching. For subcutaneous xenograft studies, 1×10^6 cells/100 µL were injected into subcutaneously into the right flank of mice. Treatment was initiated once tumors had reached 1mm^3 (approximately 2-3 weeks). Animals were euthanized once subcutaneous tumors grew large enough to impede movement. Erlotinib (50 or 75 mg/kg, Cayman Chemicals, Ann Arbor, MI USA) was administered through oral gavage. Tissues from mice used for survival studies were extracted, paraffin-embedded, sectioned (5 µm) and analyzed using immunohistochemistry.

Hydrogel fabrication: Briefly, ~5% of dissacharides of HA (700 kDa, LifeCore Biomedical, Chaska, MN, USA) was modified with thiol groups via the carboxlic acid. RGD peptide (GenScript, Piscataway, NJ USA) or free cysteine Sigma-Aldrich) were conjugated to

approximately 25% of maleimide groups on 20 kDa, 4-arm PEG-maleimide (Laysan Bio, Inc. Arab AL USA). Hydrogels were crosslinked via Michael-type Addition by mixing thiolated HA, 20 kDa PEG-thiol (Laysan Bio) and PEG-maleimide dissolved in HEPES buffer (pH 6.8). Linear compressive testing was performed using an Instron 5564 material testing device (Instron, Norwood, MA USA).

GBM cell culture: Primary GBM cell lines GBM39, HK301 and HK423 were used. HK301 and HK423 cells were generously provided by Dr. Harley Kornblum at UCLA. Cells (50,000/mL) were cultured in DMEM/F12 with 1xG21 (Gemini Bio, West Sacramento, CA USA), 1% penicillin/streptomycin, 50 ng/ml EGF (Peprotech, Rocky Hill, NJ USA), 20 ng/ml FGF-2 (Peprotech), and 25 µg/ml heparin (Sigma Aldrich). When gliomaspheres reached around 200 µm in diameter, they were dissociated into single cells in 1 mL of Tryple Express and filtered through 70 µm cell strainer. For hydrogel cultures, dissociated cells were resuspended in peptide-modified PEG-maleimide at 1 million cells/ml prior to mixing the HA-thiol/PEG-thiol to initiate crosslinking. Medium was replaced 4 days later. In some cases, 24 hrs after encapsulation, hydrogel cultures were soaked in live/dead assay solution (Life Technologies L3224) for 30 min at room temperature. Hydrogel cultures were then placed on coverglass and imaged using confocal microscopy (Leica SP5, Wetzlar, Germany).

Drug treatment: Encapsulated single cells were cultured in hydrogels for 1 week before treatment. Gliomasphere cultures were treated right after dissociation, as previously described(25). Erlotinib was re-constituted as a 10 mM stock solution in dimethylsulfoxide (DMSO). Erlotinib was then diluted to 1 µM in culture medium. DMSO alone was used as a vehicle (i.e., negative control). Cyclo-RGD was dissolved in PBS as 10 mM stock then dissolved in media as 50 µM. Culture medium and drug were replenished every third day.

Quantification of apoptosis: Cryopreserved hydrogel blocks were prepared and stained in parallel for each experimental repeat (n=3 individual repeats) using an antibody against cleaved poly ADP polymerase (c-PARP) and Hoechst 33342 as a nuclear counterstain. At least four images from randomly chosen locations per section were taken from least 2 sections. Data were analyzed using ImageProPlus software. The area fraction of c-PARP$^+$ to Hoescht$^+$ was defined as percentage of apoptotic cells. Only cells with nuclear co-localization of c-PARP and Hoescht were considered to be apoptotic.

For detailed procedures of hydrogel fabrication, hydrogel cryopreservation, Lentivirus preparation and transduction, mechanical characterization, Western blotting, immunohistochemistry and imaging, and flow cytometry, please refer to Supplementary Methods.

Results

Brain microenvironment facilitates resistance to EGFR inhibition

To investigate how the unique brain microenvironment influences physiology and treatment response of xenografted tumors, we transplanted patient-derived GBM cells at either intracranial or subcutaneous (dorsal flank) sites in nude mice. Once tumors

were established, mice were treated with either erlotinib or vehicle. Orthotopic transplants of both primary GBM cell lines (GBM39, HK301) responded poorly to erlotinib (**Fig. 1A, Fig. S1A-C**) despite its effectiveness in gliomasphere cultures (**Fig. S1D**). Erlotinib treatment suppressed growth of intracranially xenografted GBM39 tumors for only 10 days, after which time the tumors failed to respond (**Fig. 1A, FIG. S1C)**. In mice with orthotopically implanted HK301 tumors, erlotinib had no detectable effect on tumor growth or survival **(FIG. S1A, B)**. In contrast, erlotinib treatment inhibited growth of subcutaneously xenografted GBM39 tumors for more than 200 days before tumors exhibited acquired resistance (**Fig. 1B**). Tumors of HK301 cells could be established at orthotopic, but not subcutaneous, transplantation site, further indicating that the subcutaneous tissue microenvironment may not be amenable to GBM tumor growth.

Immunohistochemistry revealed HA presence surrounding and within intracranially xenografted tumors (**Fig. 1C**). In contrast, HA deposition was only found within tumors, and not surrounding tissue, in subcutaneous xenografts (**Fig. 1C**). Expression of phosphorylated EGFR (p-EGFR) and CD44 remained high in intracranial xenografts regardless of treatment (**Fig. 1D, Fig. S2C**). However, minimal expression was observed in subcutaneous xenografts (**Fig. S2C**). Furthermore, after erlotinib treatment, CD44 and p-EGFR expression were nearly undetectable (**Fig. 1D**). Based on these results, we posited that the ubiquitous abundance of HA in the brain ECM might contribute to faster acquisition of resistance to EGFR inhibition. This hypothesis was further supported by the observation that CD44 and p-EGFR were often co-expressed by GBM cells (**Fig. 1D, Fig. S2**).

Brain-mimetic hydrogels preserve in vivo phenotype of GBM cells

Although it is clear that the brain ECM contributes to characteristic multi-drug resistance in GBM (8,13,21), specific mechanisms have been difficult to uncover using conventional methods. To address current experimental limitations, we developed brain-mimetic biomaterials as 3D culture platforms to maintain the physiology of patient-derived GBM cells. Hydrogel biomaterials were fabricated so that multiple aspects of the local ECM – including HA concentration, mechanical properties and integrin-binding peptides – could be varied independently (**Fig. 2A**).

Given its potential importance for maintaining CD44 expression and resistance to EGFR inhibition (**Fig. 1**), HA was chosen as a base for hydrogel fabrication. High molecular weight HA (~700 kDa), which induces CD44 clustering to achieve distinct biological effects from its low molecular weight counterparts(26), was used to best mimic the native brain ECM. HA was modified with thiol groups to enable crosslinking via maleimide groups on polyethylene glycol (PEG) macromers. Thiol groups were conjugated to ~5% of HA disaccharides through carboxylates on N-glucuronic acid (**Fig. 2B**).

Hydrogel mechanical properties were also selected to best mimic native brain, which exhibits a linear compressive modulus around 1 kPa and a shear elastic modulus around 200 Pa(16,27,28). The concentration of HA was altered independently of stiffness by substituting bioinert PEG-thiol for HA-thiol to maintain a constant total polymer content and molar ratio of thiols to maleimide groups for crosslinking (**Fig. 2A**). **Figure 2C** demonstrates that increasing total PEG concentration from 0.5% (w/v) to 1% (w/v) yields hydrogels that are twice as stiff – 1 kPa (1173±77 Pa) and 2 kPa (2160±48 Pa) linear compressive moduli, respectively – while keeping HA concentration constant at 0.5% (w/v). In addition, HA concentration was lowered to 0.1% (w/v) while maintaining a linear compressive modulus of 1kPa (981±141 Pa). Hereafter, the mechanical properties of hydrogels are referred to as 1 kPa or 2 kPa.

As higher compressive moduli were achieved by increasing total polymer content, there remained a possibility that diffusion of key molecules, such as erlotinib and growth factors, would vary between softer and stiffer hydrogels and skew results. To evaluate this possibility, diffusion of fluorescent dye-labeled dextrans of varying molecular weights through hydrogels was quantified (**Fig. 2D**). For 20 kDa and 70 kDa dextrans, effective diffusion through the 1 kPa and 2 kPa hydrogels were statistically equivalent. For all hydrogels formulations, diffusive equilibrium (i.e., M_t/M_{inf}) was reached by around 7 hrs for 20 kDa and around 11 hrs for 70 kDa dextrans. An upper size limit was found at 150 kDa, which did not diffuse into any of the hydrogels. This result indicates that the hydrodynamic radius of 150 kDa dextran is larger than hydrogel mesh size. Results confirm that availability of nutrients, bFGF and EGF (less than 15 kDa), and erlotinib (~300 Da), was equivalent for all hydrogel cultures investigated.

GBM cell lines (HK301, GBM39, HK423), isolated from three individual patients, were investigated. All three lines were highly susceptible to erlotinib treatment when cultured as gliomaspheres (**Fig. S1D**). Gliomaspheres were dissociated into single cells and suspended in hydrogel precursor solution immediately prior to crosslinking. A live/dead assay performed 24 hrs after cell encapsulation confirmed that the majority of cells remained viable in all hydrogel conditions (**Fig. 3A, Fig. S1F**). Using an EDU-based assay to quantify numbers of proliferating cells, we found that ~20% more HK301 cells entered S-phase within a 2.5 hr period when cultured in 3D than when cultured as gliomaspheres ($p<0.05$) (**Fig. 3B**). Variations in HA content or compressive modulus had no significant effects on cell proliferation.

Basal levels of CD44 were cell line-dependent. For example, CD44 was observed on HK423 cells in all conditions, but was only detectable on HK301 cells when cultured in high HA-content hydrogels. For all cell lines evaluated, culture in hydrogels with high HA (0.5% w/v) induced increased CD44 expression compared to culture in hydrogels with low HA (0.1% w/v) or gliomaspheres (**Fig. 3C, Fig. S3**). These findings agree with our *in vivo* results, where murine xenografts robustly express CD44 when seeded in the HA-rich brain, but not at subcutaneous sites. (**Fig. 1D, Fig. S2**). Hydrogel modulus had no effects on CD44 expression (**Fig. 3C**).

GBM cells in brain-mimetic hydrogels rapidly acquire drug resistance

Effects of erlotinib treatment on GBM cells cultured in hydrogels or gliomaspheres were investigated. To mimic brain tissue(27,29), hydrogels with 0.5% (w/v) HA and 1 kPa compressive modulus were used. To characterize the cytotoxic effects of erlotinib, numbers of cells positive for nuclear cleaved poly ADP polymerase (c-PARP) were counted (**Fig. 4A**). By the 6^{th} day of treatment, GBM cells cultured within hydrogels displayed levels of apoptosis indistinguishable from non-treated controls (**Fig. 4B**). Gliomasphere cultures had significantly more apoptotic cells when treated with erlotinib **(Fig. 4B)**. In contrast to gliomasphere cultures, after 12 days of treatment GBM cells cultured within hydrogels also had acquired resistance to the cytostatic effects of erlotinib (**Fig. 4C**). In addition to erlotinib, acquisition of resistance to EGFR inhibition in hydrogels was observed when cells were treated with lapatinib (**Fig. S1G**).

Further investigation confirmed nearly complete inhibition of wild-type EGFR phosphorylation (p-wtEGFR) in gliomasphere cultures by day 3 of erlotinib treatment (**Fig. 5A,B**). In contrast, erlotinib only partially inhibited p-wtEGFR in hydrogel-cultured cells. Furthermore, erlotinib treatment increased total wtEGFR expression in both hydrogel and gliomasphere cultures (**Fig. 5A,B**). Given the high rate of cell death in erlotinib-treated, low HA (0.1% w/v) hydrogel cultures, we were not able to obtain sufficient protein lysate to perform Western blots. However, immunostaining demonstrated that higher HA content in hydrogels corresponded to increased p-EGFR expression in cultured cells (**Fig. S3**). CD44 expression also increased with HA content and, like xenografted tumors (**Fig. 1D**, **Fig. S2**), generally overlapped areas of p-EGFR expression (**Fig. S3**).

While HK423 cells express only wtEGFR and not the truncated and constitutively activate mutant, EGFRvIII, HK301 cells express both wtEGFR and EGFRvIII and GBM39 cells express only EGFRvIII (**Fig. S1E**). Although erlotinib-treated HK301 cells cultured in gliomaspheres or hydrogels upregulated total expression of wtEGFR (**Fig. 5A,B**), only in hydrogel cultures was p-EGFRvIII increased. Likewise for HK423 cells, erlotinib treatment induced higher total wt-EGFR levels in hydrogel and gliomasphere. While erlotinib treatment did attenuate p-wtEGFR in HK423 cells cultured in hydrogels or gliomaspheres, this effect was only partial in hydrogel cultures. As with HK301 cells, GBM39 cells cultured in HA hydrogels increased p-EGFRvIII (**Fig. 5A,B**). While erlotinib treatment reduced p-EGFRvIII, levels remained higher than treated gliomaspheres. In all three cell lines when treated, p-EGFR levels were always significantly higher when cultured in HA hydrogel than gliomasphere cultures **(Fig.5A,B)**.

Downstream pathways of EGFR include PI3K-AKT and MAPK-ERK, both of which many studies have reported maintain survival and growth potential of GBM tumors(3). Thus, we characterized the effects of erlotinib treatment on phosphorylation of AKT and ERK1/2 (**Fig. 5A,C**). For all 3 cell lines, culture in HA hydrogels increased p-AKT levels compared to gliomaspheres. While p-AKT levels were not altered significantly in erlotinib-treated gliomaspheres, p-AKT levels significantly increased in hydrogel-

cultured HK301 and HK423 cells (**Fig. 5A,C**). In HK301 gliomaspheres, erlotinib treatment significantly decreased p-ERK levels. Although not statistically significant, a similar trend was observed for HK423 and GBM39 gliomaspheres (**Fig. 5A,C**). In all hydrogel cultures, erlotinib treatment had no significant effects on p-ERK and p-ERK levels were significantly higher than in erlotinib-treated gliomaspheres (**Fig. 5A,C**).

Biomaterials to quantify effects of ECM cues on drug resistance

Figures 1–4 suggest that CD44 expression and HA content support the ability of GBM cells to gain erlotinib resistance. Others have reported that the mechanical microenvironment contributes to GBM tumor progression (16,24). Unlike gliomaspheres, biomaterial platforms also provide a defined, 3D mechanical environment to cultured cells. Thus, we explored the cooperative influence of hydrogel compressive modulus and HA content on acquisition of resistance to EGFR inhibition via erlotinib. Importantly, mechanical modulus was varied independently of HA concentration, so that the individual and combined contributions of each were experimentally decoupled.

Patient-derived GBM cells (HK301) were cultured in HA hydrogels to characterize the independent effects of HA concentration and compressive modulus on response to erlotinib. Total numbers of cells were tracked using bioluminescence imaging of live cultures transduced to constitutively express firefly luciferase. Results demonstrate that cells cultured in 3D hydrogels with a higher HA concentration (0.5% w/v) and lower compressive modulus (1 kPa) gained resistance to erlotinib by the 9^{th} day of treatment (**Fig. 6A**). By the 15^{th} day of treatment, there were more total cells in erlotinib-treated than untreated cultures, indicating that erlotinib-resistant cells proliferate faster. GBM cells cultured in hydrogels with high HA content (0.5% w/v), but with a stiffer modulus (2 kPa), also acquired some resistance to erlotinib; however, not until the 12^{th} day of treatment. In addition, cell numbers in treated cultures remained only ~50% of those in non-treated cultures after 15 days. Finally, GBM cells cultured in soft hydrogels (1 kPa) with a low HA concentration (0.1% w/v) did not acquire erlotinib resistance within 15 days. Instead their response was comparable to that of gliomasphere cultures, with bioluminescence signals close to background on the 15^{th} day of treatment. Furthermore, minimal HA was observed in cultured gliomaspheres (**Fig. S4C**). Together, these results indicate that high HA content was required for acquisition of resistance.

Cytotoxic and cytostatic effects of erlotinib treatment on GBM cells cultured in hydrogels were evaluated. Erlotinib-treated cells cultured in soft hydrogels (1 kPa) with high HA content (0.5% w/v) proliferated significantly faster than their untreated controls at the 3- and 6-day time points (**Fig. 6B**). This increase in proliferation correlated to the increased total numbers of viable cells observed by the 12^{th} day of treatment (**Fig. 6A**). Erlotinib treatment also induced a slight increase in cell proliferation on the 3^{rd} day in other hydrogel conditions (**Fig. 6B**). While proliferation had decreased by the 6^{th} day of treatment in all conditions, it remained elevated in 3D hydrogel cultures compared to gliomaspheres. Finally, only GBM cells cultured in soft, high HA hydrogels had escaped the cytotoxic effects of erlotinib on the 6^{th} day of treatment (**Fig. 6C**). Notably, the

kinetics of resistance acquisition to erlotinib of GBM cells cultured in soft, high HA hydrogels (**Fig. 6**) were comparable to those observed in patient-matched orthotopic xenografts in mice (**Fig. 1A**).

To further investigate the role of CD44, we used shRNA lentivirus to knockdown CD44 expression (**Fig. S4A**) and repeated erlotinib-treatment experiments. Lack of CD44 mitigated both cytotoxic and cytostatic resistance to erlotinib (**Fig. 6D,E**). Despite restoration of erlotinib efficacy for the first 6 days of treatment, even cells lacking CD44 expression gained resistance to the cytostatic effects of erlotinib by the 12^{th} day of treatment (**Fig. 6E**, **Fig. S6**). Although CD44 is a major receptor for HA, other HA receptors, such as CD168, may act to compensate for lost CD44 activity and facilitate delayed acquisition of erlotinib resistance. In soft, high HA hydrogel cultures, we observed a unique pattern of CD168 expression around the edges of cell masses resembling that of CD44 (**Fig. S4B**). In low HA hydrogels, CD168 expression was confined to the nucleus, where it participates in formation of mitotic spindles(30).

RGD and HA cooperate to evade erlotinib-induced apoptosis

Like CD44, integrins can relay both biochemical and mechanical cues through activation of FAK-PI3K-AKT and MAPK-ERK pathways – all previously implicated as mediators of resistance to treatment in GBM(16,23,24). To investigate cooperative interactions with HA-bound CD44, the ubiquitous integrin-binding sequence RGD was incorporated into hydrogel platforms (**Fig. 2A**). First, incorporation of RGD peptides into in soft hydrogels (1 kPa) with high HA content (0.5% w/v) facilitated GBM cell spreading out of spheroidal masses into the surrounding hydrogel (**Fig. 7A, Fig. S7A**). Next, we investigated how RGD incorporation into hydrogels affected cytotoxic effects of erlotinib treatment. On the 3^{rd} day of treatment, GBM cells cultured in high HA (0.5% w/v) hydrogels with RGD provided significant protection against erlotinib-induced apoptosis compared to those in high HA hydrogels without RGD or low HA (0.1% w/v) hydrogels with RGD (**Fig. 7B**). These results imply that engagement of integrin and HA receptors cooperate to amplify resistance to EGFR inhibition.

To investigate downstream effects of integrin engagement, we investigated phosphorylation of zyxin and FAK – prominent signaling proteins associated with integrin activation. When cultured in high HA hydrogels containing RGD, GBM cells upregulated p-zyxin (**Fig. 7C**). This result is not unexpected given the role of zyxin in integrin-mediated cell spreading and migration in 3D culture(31) and the invasive morphology of cells cultured in 3D hydrogels (**Fig. 7A**). However, erlotinib treatment did not affect p-zyxin levels in HK301 or HK423 cells **(Fig 7C, Fig. S7B)**.

Integrin activation of FAK is thought to facilitate cancer cell resistance to drug-induced apoptosis(15). Levels of p-FAK were similar in untreated cultures in HA hydrogels with or without RGD. However, when cultured in hydrogels containing RGD, erlotinib treatment increased p-FAK activity (**Fig. 7C, Fig. S7B**). To further confirm that apoptotic resistance was mediated by cell-RGD interactions, cyclo-RGD was used as an

inhibitor(17). Addition of cyclo-RGD effectively reversed cell spreading (**Fig. 7D**) and reduced p-zyxin (**Fig. 7E, Fig. S7B**). When treated with erlotinib and cyclo-RGD, p-FAK levels were comparable to non-treated cells (**Fig. 7E, Fig. S7B**). Moreover, this combined treatment reversed the ability of RGD to rescue cells from erlotinib-induced apoptosis (**Fig. 7F)**.

Discussion

Therapeutic resistance plays a critical role in GBM lethality. However, preclinical studies have inadequately accounted for the influence of the unique properties of brain tissue. Here, we report a biomaterial platform for 3D culture of primary GBM cells that mimics native brain tissue. In agreement previous reports, our investigations found that the ECM surrounding brain tumors is enriched in HA(32). Moreover, our data demonstrate that GBM tumors xenografted at non-CNS anatomical sites, which contain less HA in their ECM, are acquiring resistance to RTK inhibition on a much longer time scale (**Fig. 1**). Orthogonal tuning of biomaterial features revealed that an HA-rich, mechanically soft culture environment is required for GBM cells to acquire resistance to RTK inhibition (**Fig. 6A**). Furthermore, 3D cultures of patient-derived GBM cells in biomaterials with defined HA content and mechanical properties rapidly developed resistance to erlotinib in a manner consistent with patient-matched mouse xenografts (**Fig. 1, Fig. 6, Fig. S1A**) and clinical reports(6). Specifically, in both orthotopic animal and high HA hydrogel experimental settings, GBM cells acquired erlotinib resistance between 9 and 12 days of treatment. Taken together, results demonstrate the utility of these biomaterial cultures as *ex vivo* models of GBM that better recapitulate the brain microenvironment than standard culture methods yet are easier, more affordable, less time consuming (days versus weeks to establish tumors) and provide a more controlled experimental context than animal models.

For all primary GBM cell lines evaluated, changes in cytotoxic and cytostatic effects of erlotinib over time were consistent with acquisition of resistance – where despite an initial inhibition of p-EGFR, treatment reduced apoptosis while increasing proliferation (**Fig. 4,5**). 3D culture in HA-rich hydrogels alone increased p-AKT, while erlotinib treatment further upregulated p-AKT levels (**Fig. 5A,C**). This finding indicates that GBM cells resistant to EGFR inhibition may be more aggressive – a possible explanation of increased proliferation in HK301 after treatment in high HA hydrogel (**Fig. 5A,C, Fig. 6B**). In addition to EGFR inhibition via the small molecule erlotinib, hydrogel-cultured GBM cells gained resistance to lapatinib – another RTK inhibitor – providing evidence that culture of primary GBM cells in 3D brain-mimetic biomaterials represent a clinically relevant method for evaluate drug response (**Fig. S1G**).

Here, we implemented several key improvements over previously reported HA-based biomaterials for 3D cell culture(24,33–37) that enabled development of culture platforms representing a compelling new preclinical model for studying mechanisms of drug resistance in brain cancers. First, HA was minimally modified (~5% of disaccharides contain a thiol substitution) to maintain the native ability of high molecular weight HA to

interact with CD44 receptors(38). In contrast, other methods often modify up to 70% of HA disaccharides.

Second, while previous methods have relied on HA polysaccharides with molecular weights at or below 200 kDa, we incorporated HA with a range of molecular weights from 500–750 kDa. This size difference has significant effects on HA bioactivity(26,39). For example, while high molecular weight HA (500–1000 kDa), which is found in abundance in native brain, suppresses the immune system, 200 kDa HA stimulates cytokine production(26). High molecular weight HA has also been reported to activate RTKs more efficiently than smaller HA chains(39). Although some HA is detected in subcutaneously implanted GBM tumors, it is thought that tumors contain high amounts of low molecular weight of HA, which contribute to tumor growth and angiogenesis (40).

Third, the biomaterial platforms reported here achieved effective decoupling of HA content, stiffness, availability of integrin-binding sites and diffusion. Previously reported methods for HA hydrogel fabrication typically increased hydrogel stiffness by increasing HA concentration, and thus total polymer content(27,34). Another common method substitutes gelatin to vary HA concentration without altering total polymer content; however, gelatin contains RGD sites(36,37). In our system, orthogonal control of these variables enabled systematic investigation of how individual features interact to facilitate acquisition of treatment resistance.

Finally, the majority of previous studies of GBM in 3D biomaterial models have explored only immortalized cells lines, such as U87 cells, which likely have significant phenotypic deviations from primary, patient-isolated GBM cells(41). Although logistically more challenging, primary GBM cells – as used here – are more likely to yield clinically translatable findings. Moreover, compatibility of an *ex vivo* experimental platform with primary GBM cells isolated from multiple patients will facilitate future application to personalized medicine.

The lack of CD44 expression in hydrogel cultures with lower HA content (**Fig. 3C**, **Fig. S3**) indicates HA may induce upregulation of CD44 receptors that can then respond to mechanical cues. Previous studies have shown that mechanical cues are transduced through the PI3K-AKT pathway, despite EGFR inhibition(22). This may explain why EGFR resistance is more pronounced in GBM cultures with comparable HA levels and CD44 expression, but different mechanical moduli. As knockdown of CD44 restored the cytostatic and cytotoxic effects of erlotinib, we are confident that HA-CD44 interactions contributed to acquisition of erlotinib resistance (**Fig. 6D, E**). However, cytostatic effects were lost over time – implying that GBM cells eventually acquired resistance through a CD44-independent mechanism. Our observation that the CD168 receptor was highly expressed at the cell membrane in these cultures (**Fig. S4B**) suggests that CD168-HA interactions may compensate for the loss of CD44 to permit acquisition of erlotinib resistance.

Our results are in agreement with previous reports that HA-bound CD44 facilitates activation of wtEGFR, and thus resistance to EGFR inhibition(22,39,42) **(Fig. 5A,B, Fig. S3**). The observations that areas of CD44 and p-EGFR expression overlap in GBM cells cultured in HA-rich hydrogels (**Fig. 3C, Fig. S3**) and tumors xenografted in HA-rich brain (**Fig. 1D, Fig. S2**) indicate that HA-bound CD44 may increase activation of EGFR through physical interactions at the cell membrane and facilitate resistance to EGFR inhibition. This has been previously reported to occur in orthotopic xenografts and clinical samples(22,42). CD44 may also effect activation of EGFRvIII. a common variant in clinical tumors associated with resistance to EGFR inhibition and worse patient outcomes(2,25,43). Notably, RGD peptides into acted synergistically with HA in hydrogels to induce cell spreading and protect GBM cells from erlotinib-induced apoptosis (**Fig. 7B**). These results imply that a combination therapy of integrin, CD44 and EGFR inhibition may have clinical potential.

Given the complexity of GBM tumors *in vivo* – including powerful cooperative mechanisms and the presence of confounding variables such as the blood-brain barrier – it has been challenging to isolate the contributions of individual ECM features using animal models. On the other hand, standard *in vitro* culture methods do not account for key features of the brain ECM that are crucial to preserving tumor physiology and obtaining experimental results with clinical relevance. Here, we describe biomaterial platforms that recapitulate the brain microenvironment to produce *ex vivo* cultures of primary GBM cell lines with unique genetic and phenotypic profiles that are physiologically representative of clinical tumors. Specifically, mechanisms and kinetics of acquisition of resistance to EGFR inhibition were preserved in biomaterial, but not in standard gliomasphere cultures. Compared to animal models, these biomaterial scaffolds provide researchers with a platform in which to perform highly controlled experiments faster, cheaper and more reproducibly. In addition, scaffolds are optically transparent – permitting imaging of 3D cultures – and compatible with standard techniques for tissue processing – including sectioning and histological staining. The ability to independently vary individual parameters within the ECM enables characterization of how multiple ECM cues act together to facilitate acquisition of treatment resistance and amplify aggressive characteristics. Here, this function was used to demonstrate how mechanical modulus, HA content and RGD peptides mediate acquisition of resistance to RTK inhibition through cooperative interactions among HA, CD44, integrins and EGFR. In conclusion, these biomimetic scaffolds with orthogonal control over ECM parameters provide a unique tool for researchers to better understand how the complex microenvironment in GBM tumors fuels treatment resistance and cancer progression.

Acknowledgements: This work was supported with funding from the NIH (R21NS093199) and the UCLA ARC 3R's Award. We thank UCLA Tissue Pathology Core Laboratory (TPCL) for cryosectioning, Advanced Light Microscopy/Spectroscopy core facility (ALMS) in California Nanosystems Institute (CNSI) at UCLA for use of the confocal microscope, UCLA Crump Institute for Molecular Imaging for using IVIS

imaging system, Dr. Benjamin Wu Lab in department of bioengineering at UCLA for providing Instron instrument, UCLA Molecular Instrumentation Center (MIC) for providing magnetic resonance spectroscopy, and Flow Cytometry Core in Jonsson Comprehensive Cancer Center (JCCC) at UCLA for providing instrumentation for flow cytometry. Monoclonal antibody against CD44 clone H4C4 developed by August, J.T./Hildreth, J.E.K. was obtained from the Developmental Studies Hybridoma Bank, created by NICHD of the NIH and maintained at the University of Iowa, Department of Biology, Iowa City, IA 52242.

Author Contributions: W.X. contributed to experimental design, performance of all experiments, data analysis and manuscript preparation. A.S. and A.E. contributed to hydrogel fabrication and characterization. R.Z., S.S., J.L. and C.W. helped perform *in vitro* experiments. L.T. performed animal experiments. S.K.S. and D.A.N. contributed to experimental design, data analysis and manuscript preparation.

1. Ostrom QT, Gittleman H, Farah P, Ondracek A, Chen Y, Wolinsky Y, et al. CBTRUS statistical report: Primary brain and central nervous system tumors diagnosed in the United States in 2006 - 2010. J Neurooncol. 2013;15:788–96.

2. Furnari FB, Cloughesy TF, Cavenee WK, Mischel PS. Heterogeneity of epidermal growth factor receptor signalling networks in glioblastoma. Nat Rev Cancer [Internet]. 2015;15:302–10. Available from: http://www.nature.com/doifinder/10.1038/nrc3918

3. E Taylor T, B Furnari F, K Cavenee W. Targeting EGFR for treatment of glioblastoma: molecular basis to overcome resistance. Curr Cancer Drug Targets. Bentham Science Publishers; 2012;12:197–209.

4. Shepherd FA, Rodrigues Pereira J, Ciuleanu T, Tan EH, Hirsh V, Thongprasert S, et al. Erlotinib in Previously Treated Non–Small-Cell Lung Cancer. N Engl J Med [Internet]. 2005;353:123–32. Available from: http://www.nejm.org/doi/abs/10.1056/NEJMoa050753

5. Slamon DJ, Leyland-Jones B, Shak S, Fuchs H, Paton V, Bajamonde A, et al. Use of chemotherapy plus a monoclonal antibody against HER2 for metastatic breast cancer that overexpresses HER2. N Engl J Med. Mass Medical Soc; 2001;344:783–92.

6. Brandes AA, Franceschi E, Tosoni A, Hegi ME, Stupp R. Epidermal growth factor receptor inhibitors in neuro-oncology: hopes and disappointments. Clin Cancer Res. AACR; 2008;14:957–60.

7. Bernstein JJ, Woodard CA. Glioblastoma cells do not intravasate into blood vessels. Neurosurgery. LWW; 1995;36:124–32.

8. Gilg AG, Tye SL, Tolliver LB, Wheeler WG, Visconti RP, Duncan JD, et al. Targeting hyaluronan interactions in malignant gliomas and their drug-resistant multipotent progenitors. Clin Cancer Res. AACR; 2008;14:1804–13.

9. Tilghman J, Wu H, Sang Y, Shi X, Guerrero-Cazares H, Quinones-Hinojosa A, et al. HMMR maintains the stemness and tumorigenicity of glioblastoma stem-like

cells. Cancer Res. AACR; 2014;74:3168–79.

10. Pietras A, Katz AM, Ekström EJ, Wee B, Halliday JJ, Pitter KL, et al. Osteopontin-CD44 signaling in the glioma perivascular niche enhances cancer stem cell phenotypes and promotes aggressive tumor growth. Cell Stem Cell. Elsevier; 2014;14:357–69.

11. Lathia JD, Mack SC, Mulkearns-Hubert EE, Valentim CLL, Rich JN. Cancer stem cells in glioblastoma. Genes Dev. Cold Spring Harbor Lab; 2015;29:1203–17.

12. Ranuncolo SM, Ladeda V, Specterman S, Varela M, Lastiri J, Morandi A, et al. CD44 expression in human gliomas. J Surg Oncol. Wiley Online Library; 2002;79:30–6.

13. Gladson CL. The extracellular matrix of gliomas: modulation of cell function. J Neuropathol Exp Neurol. LWW; 1999;58:1029–40.

14. Mahesparan R, Read T-A, Lund-Johansen M, Skaftnesmo K, Bjerkvig R, Engebraaten O. Expression of extracellular matrix components in a highly infiltrative in vivo glioma model. Acta Neuropathol. Springer; 2003;105:49–57.

15. Guo W, Giancotti FG. Integrin signalling during tumour progression. Nat Rev Mol Cell Biol. Nature Publishing Group; 2004;5:816.

16. Miroshnikova YA, Mouw JK, Barnes JM, Pickup MW, Lakins JN, Kim Y, et al. Tissue mechanics promote IDH1-dependent HIF1α-tenascin C feedback to regulate glioblastoma aggression. Nat Cell Biol. 2016;18:1336–45.

17. Reardon DA, Neyns B, Weller M, Tonn JC, Nabors LB, Stupp R. Cilengitide: an RGD pentapeptide αvβ3 and αvβ5 integrin inhibitor in development for glioblastoma and other malignancies. Futur Oncol. Future Medicine; 2011;7:339–54.

18. Wang SJ, Bourguignon LYW. Hyaluronan and the interaction between CD44 and epidermal growth factor receptor in oncogenic signaling and chemotherapy resistance in head and neck cancer. Arch Otolaryngol Neck Surg. American Medical Association; 2006;132:771–8.

19. Lee J-L, Wang M-J, Sudhir P-R, Chen J-Y. CD44 engagement promotes matrix-derived survival through the CD44-SRC-integrin axis in lipid rafts. Mol Cell Biol. Am Soc Microbiol; 2008;28:5710–23.

20. Lee J-L, Wang M-J, Sudhir P-R, Chen G-D, Chi C-W, Chen J-Y. Osteopontin promotes integrin activation through outside-in and inside-out mechanisms: OPN-CD44V interaction enhances survival in gastrointestinal cancer cells. Cancer Res. AACR; 2007;67:2089–97.

21. Zustiak SP, Dadhwal S, Medina C, Steczina S, Chehreghanianzabi Y, Ashraf A, et al. Three- dimensional matrix stiffness and adhesive ligands affect cancer cell response to toxins. Biotechnol Bioeng. Wiley Online Library; 2016;113:443–52.

22. Herishanu Y, Gibellini F, Njuguna N, Hazan-Halevy I, Keyvanfar K, Lee E, et al.

CD44 signaling via PI3K/AKT and MAPK/ERK pathways protects CLL cells from spontaneous and drug induced apoptosis through MCL-1. Leuk Lymphoma. NIH Public Access; 2011;52:1758.

23. Chopra A, Murray ME, Byfield FJ, Mendez MG, Halleluyan R, Restle DJ, et al. Augmentation of integrin-mediated mechanotransduction by hyaluronic acid. Biomaterials. Elsevier; 2014;35:71–82.

24. Kim Y, Kumar S. CD44-mediated adhesion to hyaluronic acid contributes to mechanosensing and invasive motility. Mol Cancer Res. AACR; 2014;12:1416–29.

25. Nathanson DA, Gini B, Mottahedeh J, Visnyei K, Koga T, Gomez G, et al. Targeted therapy resistance mediated by dynamic regulation of extrachromosomal mutant EGFR DNA. Science (80-). American Association for the Advancement of Science; 2014;343:72–6.

26. Stern R, Asari AA, Sugahara KN. Hyaluronan fragments: an information-rich system. Eur J Cell Biol. Elsevier; 2006;85:699–715.

27. Seidlits SK, Khaing ZZ, Petersen RR, Nickels JD, Vanscoy JE, Shear JB, et al. The effects of hyaluronic acid hydrogels with tunable mechanical properties on neural progenitor cell differentiation. Biomaterials. Elsevier; 2010;31:3930–40.

28. Georges PC, Miller WJ, Meaney DF, Sawyer ES, Janmey PA. Matrices with compliance comparable to that of brain tissue select neuronal over glial growth in mixed cortical cultures. Biophys J. Elsevier; 2006;90:3012–8.

29. Armstrong SE, Bell DR. Measurement of high-molecular-weight hyaluronan in solid tissue using agarose gel electrophoresis. Anal Biochem. Elsevier; 2002;308:255–64.

30. Telmer PG, Tolg C, McCarthy JB, Turley EA. How does a protein with dual mitotic spindle and extracellular matrix receptor functions affect tumor susceptibility and progression? Commun Integr Biol. Taylor & Francis; 2011;4:182–5.

31. Fraley SI, Feng Y, Giri A, Longmore GD, Wirtz D. Dimensional and temporal controls of three-dimensional cell migration by zyxin and binding partners. Nat Commun. NIH Public Access; 2012;3:719.

32. Jadin L, Pastorino S, Symons R, Nomura N, Jiang P, Juarez T, et al. Hyaluronan expression in primary and secondary brain tumors. Ann Transl Med. 2015;3.

33. Ananthanarayanan B, Kim Y, Kumar S. Elucidating the mechanobiology of malignant brain tumors using a brain matrix-mimetic hyaluronic acid hydrogel platform. Biomaterials. Elsevier; 2011;32:7913–23.

34. Heffernan JM, Overstreet DJ, Le LD, Vernon BL, Sirianni RW. Bioengineered scaffolds for 3D analysis of glioblastoma proliferation and invasion. Ann Biomed Eng. Springer; 2015;43:1965–77.

35. Wang C, Tong X, Yang F. Bioengineered 3D brain tumor model to elucidate the effects of matrix stiffness on glioblastoma cell behavior using PEG-based

hydrogels. Mol Pharm. ACS Publications; 2014;11:2115–25.

36. Pedron S, Harley BAC. Impact of the biophysical features of a 3D gelatin microenvironment on glioblastoma malignancy. J Biomed Mater Res Part A. Wiley Online Library; 2013;101:3404–15.

37. Chen JE, Pedron S, Harley BAC. The Combined Influence of Hydrogel Stiffness and Matrix- Bound Hyaluronic Acid Content on Glioblastoma Invasion. Macromol Biosci. Wiley Online Library; 2017;

38. Hachet E, Van den Berghe H, Bayma E, Block MR, Auzély-Velty R. Design of biomimetic cell-interactive substrates using hyaluronic acid hydrogels with tunable mechanical properties. Biomacromolecules. ACS Publications; 2012;13:1818–27.

39. Lokeshwar VB, Selzer MG. Differences in hyaluronic acid-mediated functions and signaling in arterial, microvessel, and vein-derived human endothelial cells. J Biol Chem. ASBMB; 2000;275:27641–9.

40. Misra S, Hascall VC, Markwald RR, Ghatak S. Interactions between hyaluronan and its receptors (CD44, RHAMM) regulate the activities of inflammation and cancer. Front Immunol. Frontiers; 2015;6:201.

41. Lee J, Kotliarova S, Kotliarov Y, Li A, Su Q, Donin NM, et al. Tumor stem cells derived from glioblastomas cultured in bFGF and EGF more closely mirror the phenotype and genotype of primary tumors than do serum-cultured cell lines. Cancer Cell. Elsevier; 2006;9:391–403.

42. Tsatas D, Kanagasundaram V, Kaye A, Novak U. EGF receptor modifies cellular responses to hyaluronan in glioblastoma cell lines. J Clin Neurosci. Elsevier; 2002;9:282–8.

43. Shinojima N, Tada K, Shiraishi S, Kamiryo T, Kochi M, Nakamura H, et al. Prognostic value of epidermal growth factor receptor in patients with glioblastoma multiforme. Cancer Res. AACR; 2003;63:6962–70.

Figure 1. Glioblastoma xenografts acquire resistance to erlotinib at intracranial sites with faster kinetics than at subcutaneous sites. A) Bioluminescence imaging of orthotopic xenografts of GBM39 cells (normalized to day 0 before treatment with 50mg/kg erlotinib). Error bars represent standard deviation (n=3). B) Volume of subcutaneously xenografted tumors of GBM39 cells (normalized to day 0 before treatment with 50mg/kg erlotinib). Error bars represent standard deviation (n=4) C) Representative images of immunohistochemical staining for HA (brown color indicates positive stain and purple color for hematoxylin stain) of intracranial and subcutaneous xenografts of GBM39 cells. White dashed line separates tumor and brain, and black dashed separates tumor and subcutaneous area. Scale bar = 100 μm. For negative control slides for staining please refer to Supplementary Fig. S2A. D) On left, representative images of immunofluorescence staining for CD44 (red), p-EGFR (Tyr1068) (green) and Hoechst 33342 (blue) of intracranial and subcutaneous xenografts of GBM39 cells. Arrows indicate cells expressing both p-EGFR and CD44. On right, H&E image of same tissue at similar location. For negative control slides of same tissue please refer to Supplementary Fig. S2B. Scale bar = 200 μm.

Figure 2. Fabrication and characterization of biomaterial platforms. A) Schematic of hydrogel encapsulation of GBM cells for 3D culture. Cysteine-bearing peptides were first conjugated to PEG maleimide. Single GBM cells were resuspended PEG maleimide-peptide before mixing with PEG thiol and 5% thiolated HA. Molar ratio of thiol to maleimide was maintained at approximately 1.1 to 1. B) Representative H^1-NMR spectrum of thiolation, indicating that approximately 5% of HA glucuronic acid groups have been modified with a thiol. C) Linear compressive moduli of hydrogels. Percentages indicate weight to volume ratios (w/v). Error bars represent S.E.M. (n=3). One-way ANOVA with Tukey's test for multiple comparisons were performed (***$p <$ 0.001). D) Left panel shows effective diffusion coefficients (cm^2/s) for 20 kDa and 70 kDa dextrans, respectively, through hydrogels. Two-way ANOVA with Tukey's test for multiple comparisons were performed (***p<0.001). Error bars represent S.E.M. (n=3). Right panel shows diffusion over time of dextran through HA hydrogels. M_t/M_{inf} is defined as the ratio of dextran released at a specific time (M_t) to the total amount of dextran released at infinite time (M_{inf}). M_t/M_{inf} is plotted against the square root of time ($s^{1/2}$) so that the slope indicates diffusion rate. HA percentage indicates volume to weight percentage (% w/v).

Figure 3. Characterization of patient-derived GBM cells in 3D hydrogel culture. A) Representative confocal microscopy images showing live (green) and dead (red) cells 24 hours after hydrogel encapsulation of HK301 cells. Scale bar=100 μm. Lower right panel, quantification of percentage of viable cells by counting red/green staining 24 hours after encapsulation of HK301. Error bar represents S.E.M. (n=3). One-way ANOVA with Tukey's multiplicity test was performed. NS represents non-significance. B)

EdU analysis through flow cytometer. On the 4th day of culture, encapsulated cells were pulsed with EdU (1 μM) for 2.5 hours. Cells were removed from hydrogels and percentage of cells that had proliferated (EdU^{+}) assessed using a flow cytometer. One-way ANOVA with Tukey's test for multiple comparisons was performed (*p < 0.05). C) Representative images of immunofluorescence staining for CD44 (red) in cryosectioned hydrogel and gliomasphere cultures of HK301 cells. Scale bar = 100 μm. HA percentage indicates volume to weight percentage (% w/v).

Figure 4. GBM cells in 3D, HA hydrogel cultures acquire cytotoxic and cytostatic resistance to erlotinib. A) Representative images of immunofluorescence staining of cleaved polyADP polymerase (c-PARP) in HK301 cells after 6 days of erlotinib treatment. Scale bar = 200 μm. B) Quantification of apoptotic (c-PARP^{+}) after 6 days of erlotinib treatment. Error bars indicate S.E.M. (n=3). Students' t-tests were performed (*p < 0.05, **p < 0.01). C) Proliferation rate of cells (EdU incorporation over 2.5 hours) after 12 days of erlotinib treatment. Erlotinib-treated samples were normalized to non-treated samples for each condition. Students' t-test was performed (**p < 0.01). Error bars indicate S.E.M. (n=3).

Figure 5. Signaling analysis for HA cultured cells and gliomaspheres. A) Representative western blot images of 72 hours after erlotinib treatment. HA percentage indicates volume to weight percentage (% w/v). Gliomasphere (GS). B,C) integrated intensity signals of B)phospho-EGFR, C) phospho-AKT and phospho-ERK1/2 for western blot of FIG. 5A. Error bar represents standard deviation from independent repeats (HK301 (n=5), HK423 (n=4), and GBM39 (n=3)). One-way ANOVA and Tukeys's multiple comparison test was used. *p<0.05, **p<0.01, ***p<0.001, ****p<0.0001.

Figure 6. HA content and modulus contribute to kinetics of acquisition of erlotinib resistance. A) Chemiluminescent signal measured 2 hrs after addition of luciferin (1 mM). Signals of erlotinib-treated HK301 cells were normalized to non-treated samples and signal before treatment (day 0) for each condition. Two-way ANOVA (culture condition, time) with Šidák's test for multiple comparisons of hydrogel condition against gliomasphere culture were performed. Error bars show standard deviation (n=3). B) Proliferation rate of HK301 cells (EdU incorporation over 2.5 hours) during erlotinib treatment. Erlotinib-treated samples were normalized to non-treated samples for each condition. Error bars indicate S.E.M. (n=3). Two-way ANOVA (culture condition, time) with Šidák's test for multiple comparisons of hydrogel condition against gliomasphere culture were performed. C, D) Percentage of apoptotic (c-PARP^{+}) HK301 cells after 6 days of erlotinib treatment. Error bars indicate S.E.M. (n=3) One-way ANOVA with Tukey's test for multiple comparisons was performed. For representative images of cl-PARP staining, please refer to FIG. S5A. E) Proliferation rate of HK301 cells (EdU

incorporation over 2.5 hours) during erlotinib treatment. Erlotinib-treated samples were normalized to non-treated samples for each condition. Error bars indicate S.E.M. (n=3). Two-way ANOVA (cell type, time) with Šidák's test for multiple comparisons were performed. HA percentage indicates volume to weight percentage (% w/v). *$p < 0.05$, **$p < 0.01$, ****$p < 0.0001$.

Figure 7. Interactions of integrins and CD44 with the scaffold protect glioblastoma cells from erlotinib-induced apoptosis (HK301 cells). A) Representative phase contrast images of hydrogel-cultured cells 8 days after encapsulation. Scale bar = 200 µm. B) Percentage of apoptotic (c-PARP$^+$) cells after 3 days of erlotinib treatment. Error bars indicate S.E.M. (n=3). Two-way ANOVA (hydrogel condition, treatment) with Šidák's test for multiple comparisons were performed (***$p < 0.001$). C) Right panel, representative western blot images 6 days after erlotinib treatment. HK301 was encapsulated in different gel types. Left panel, Normalized integrated intensity signals of phospho-FAK (A), total-FAK and phospho-zyxin (n=4). Error bar represents standard deviation across individual experimental repeats. D) Representative images phase contrast images 3 days after treatment with cyclo-RGD (50 µM). E) Right panel, representative western blot image of HK301 cells after 6 days of treatment. Left panel, normalized integrated intensity signals of phospho-FAK and phospho-zyxin (n=4) Error bar represents standard deviation across individual experimental repeats. F) Percentage of apoptotic (c-PARP$^+$) cells 3 days after cyclo-RGD treatment. Error bars indicate S.E.M. (n=3). One-way Anova with Tukey's test for multiple comparisons were performed (*$p < 0.05$, **$p < 0.01$). HA percentage indicates volume to weight percentage (% w/v). "E" - 1µM erlotinib, "ER" - 1µM erlotinib and 50 µM cyclo-RGD, "R" - 50 µM cyclo-RGD, "V" - vehicle (DMSO or PBS). For representative staining of cl-PARP, please refer to FIG. S5B.

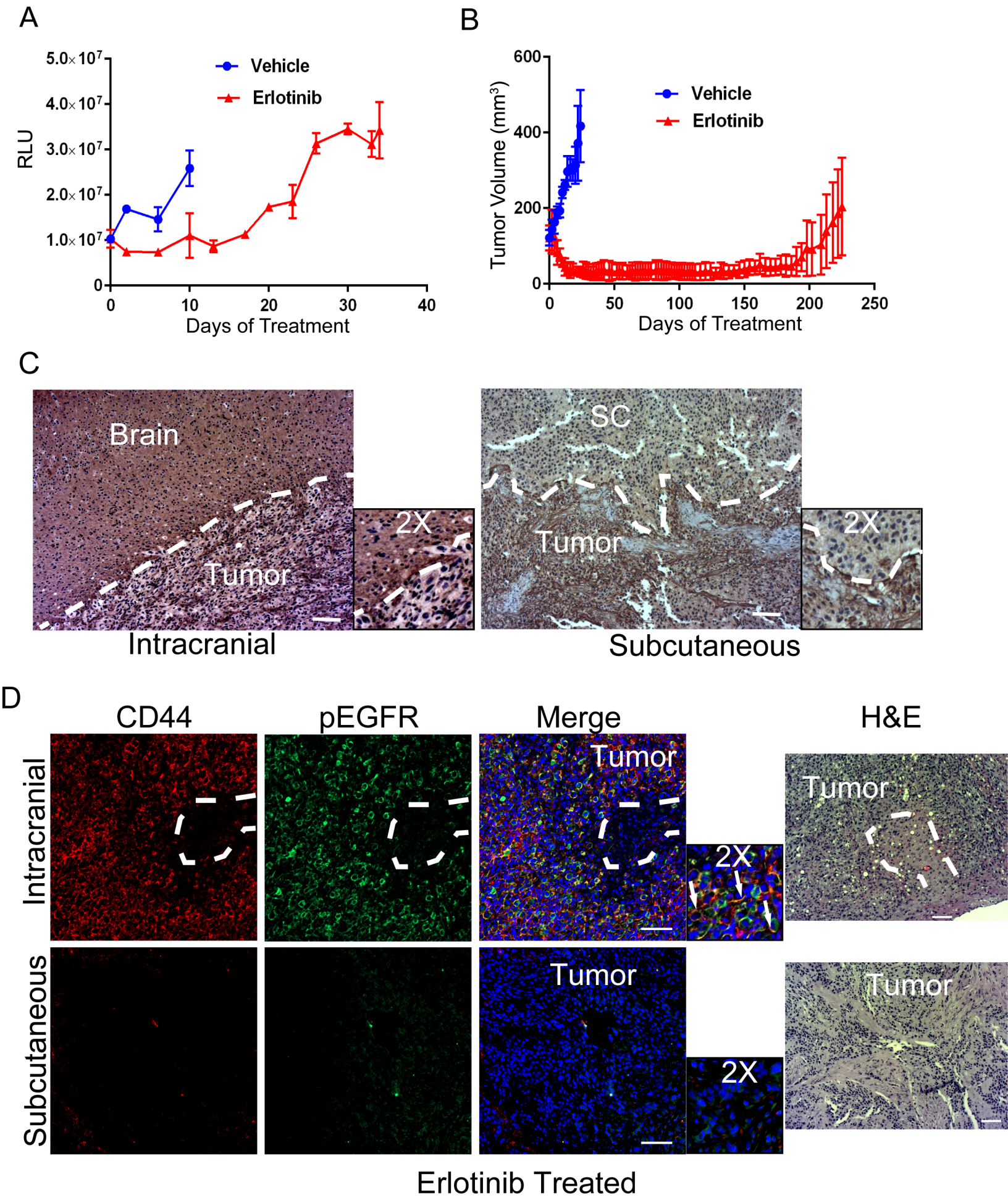
A
RLU
5.0×10^7
4.0×10^7
3.0×10^7
2.0×10^7
1.0×10^7
0
Vehicle
Erlotinib
0
10
20
30
40
Days of Treatment
B
Tumor Volume (mm^3)
600
400
200
0
Vehicle
Erlotinib
0
50
100
150
200
250
Days of Treatment
C
Brain
Tumor
2X
Intracranial
SC
Tumor
2X
Subcutaneous
D
CD44
pEGFR
Merge
H&E
Intracranial
Tumor
2X
Tumor
Subcutaneous
Tumor
2X
Tumor
Erlotinib Treated

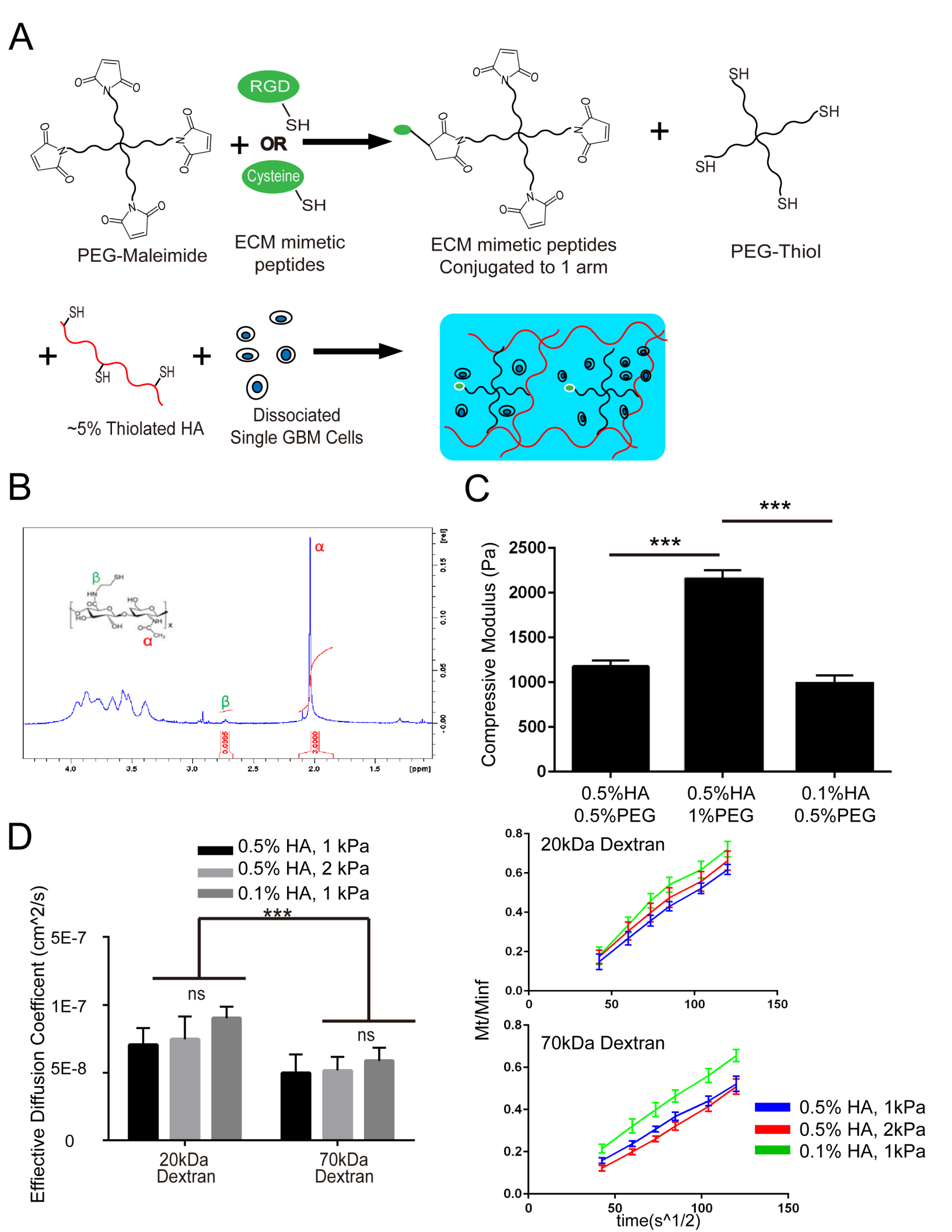
A
RGD
SH
OR
Cysteine
SH
PEG-Maleimide
ECM mimetic peptides
ECM mimetic peptides Conjugated to 1 arm
PEG-Thiol
~5% Thiolated HA
Dissociated Single GBM Cells
B
α
β
[ppm]
C
***
***
Compressive Modulus (Pa)
2500
2000
1500
1000
500
0
0.5%HA 0.5%PEG
0.5%HA 1%PEG
0.1%HA 0.5%PEG
D
0.5% HA, 1 kPa
0.5% HA, 2 kPa
0.1% HA, 1 kPa
***
ns
ns
Effective Diffusion Coefficent (cm^2/s)
5E-7
1E-7
5E-8
0
20kDa Dextran
70kDa Dextran
20kDa Dextran
70kDa Dextran
Mt/Minf
time(s^1/2)
0.5% HA, 1kPa
0.5% HA, 2kPa
0.1% HA, 1kPa

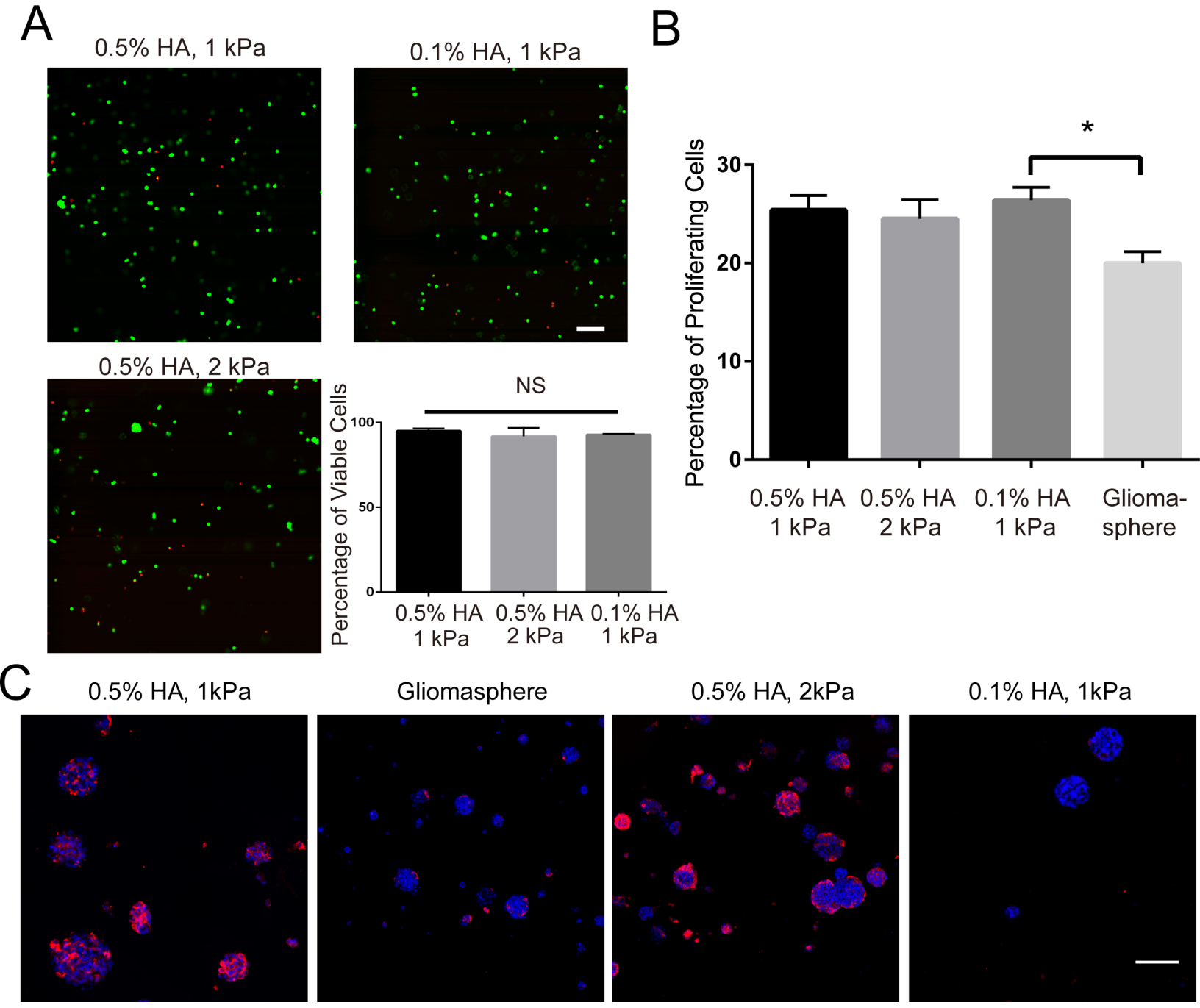
A
0.5% HA, 1 kPa
0.1% HA, 1 kPa
0.5% HA, 2 kPa
NS
Percentage of Viable Cells
100
50
0
0.5% HA 1 kPa
0.5% HA 2 kPa
0.1% HA 1 kPa
B
*
Percentage of Proliferating Cells
30
20
10
0
0.5% HA 1 kPa
0.5% HA 2 kPa
0.1% HA 1 kPa
Glioma-sphere
C
0.5% HA, 1kPa
Gliomasphere
0.5% HA, 2kPa
0.1% HA, 1kPa

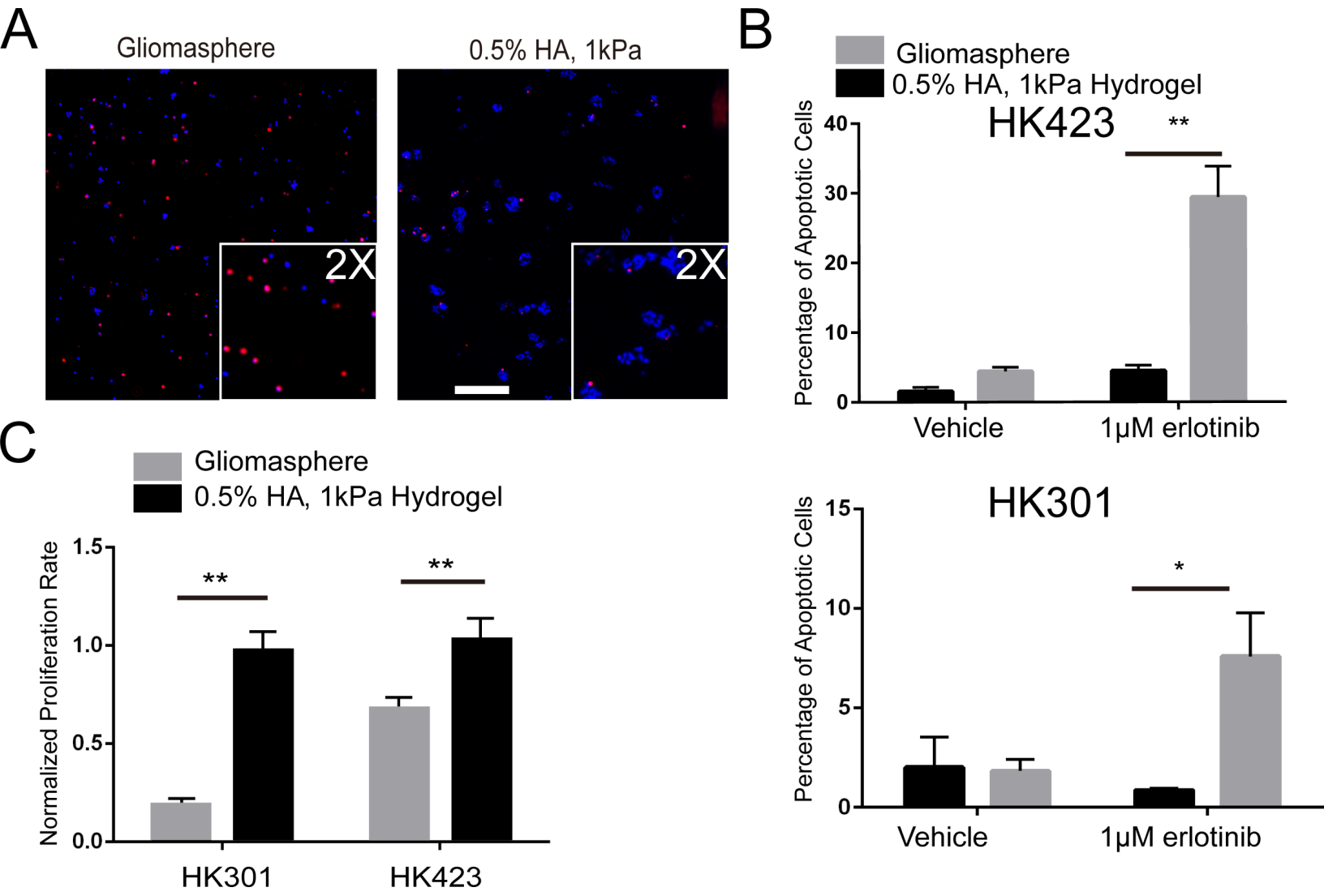
A
Gliomasphere
0.5% HA, 1kPa
2X
2X
B
Gliomasphere
0.5% HA, 1kPa Hydrogel
HK423
**
Percentage of Apoptotic Cells
40
30
20
10
0
Vehicle
1μM erlotinib
HK301
*
Percentage of Apoptotic Cells
15
10
5
0
Vehicle
1μM erlotinib
C
Gliomasphere
0.5% HA, 1kPa Hydrogel
Normalized Proliferation Rate
1.5
1.0
0.5
0.0
**
**
HK301
HK423

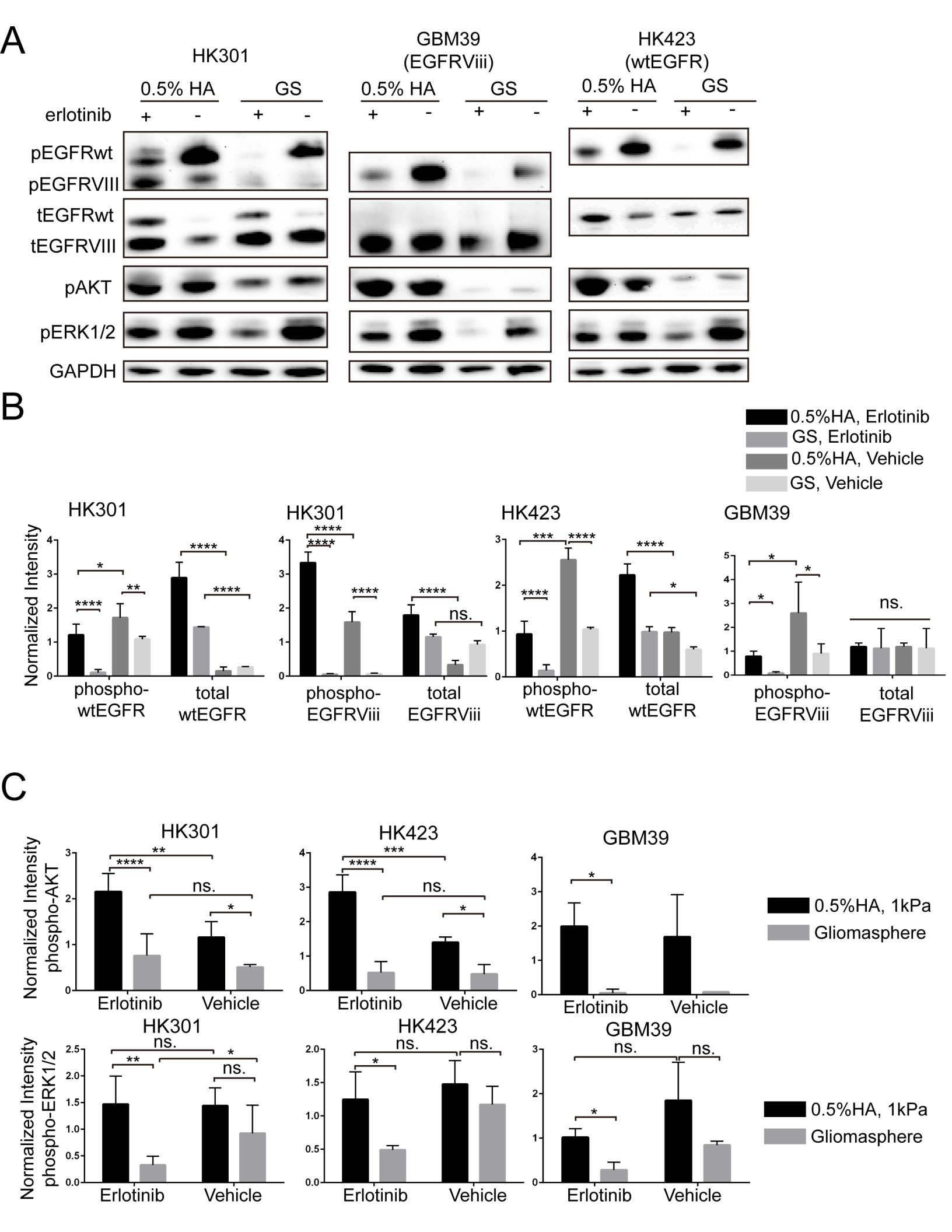
A
HK301
GBM39 (EGFRViii)
HK423 (wtEGFR)
0.5% HA
GS
erlotinib
pEGFRwt
pEGFRVIII
tEGFRwt
tEGFRVIII
pAKT
pERK1/2
GAPDH
B
0.5%HA, Erlotinib
GS, Erlotinib
0.5%HA, Vehicle
GS, Vehicle
Normalized Intensity
phospho-wtEGFR
total wtEGFR
phospho-EGFRViii
total EGFRViii
ns.
C
Normalized Intensity phospho-AKT
Normalized Intensity phospho-ERK1/2
Erlotinib
Vehicle
0.5%HA, 1kPa
Gliomasphere

A

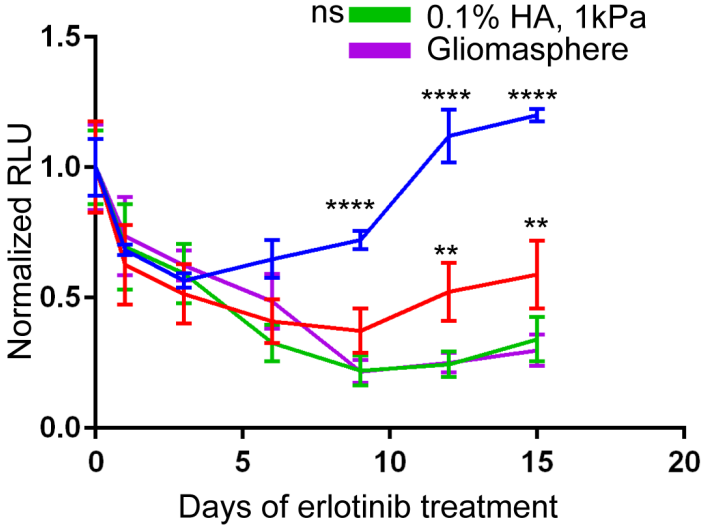
**** 0.5% HA, 1kPa
* 0.5% HA, 2kPa
ns 0.1% HA, 1kPa
Gliomasphere
Normalized RLU
Days of erlotinib treatment

B

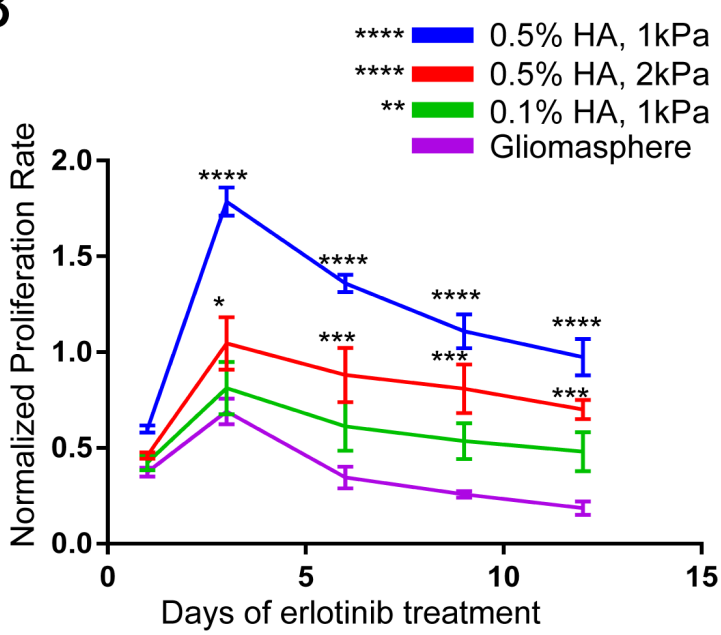
**** 0.5% HA, 1kPa
**** 0.5% HA, 2kPa
** 0.1% HA, 1kPa
Gliomasphere
Normalized Proliferation Rate
Days of erlotinib treatment

C

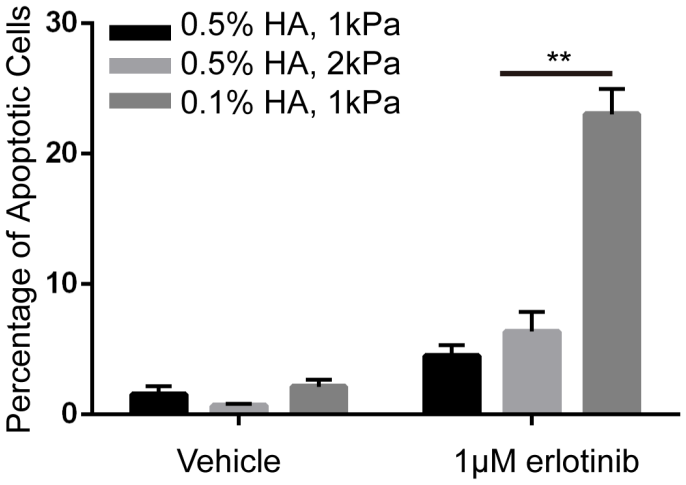
0.5% HA, 1kPa
0.5% HA, 2kPa
0.1% HA, 1kPa
Percentage of Apoptotic Cells
Vehicle
1μM erlotinib

D

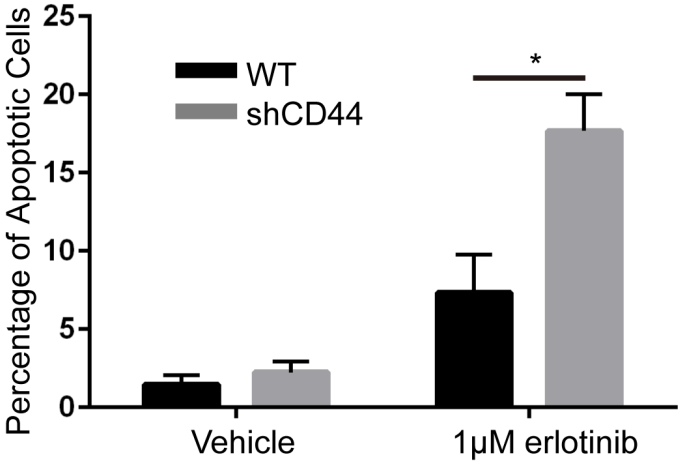
WT
shCD44
Percentage of Apoptotic Cells
Vehicle
1μM erlotinib

E

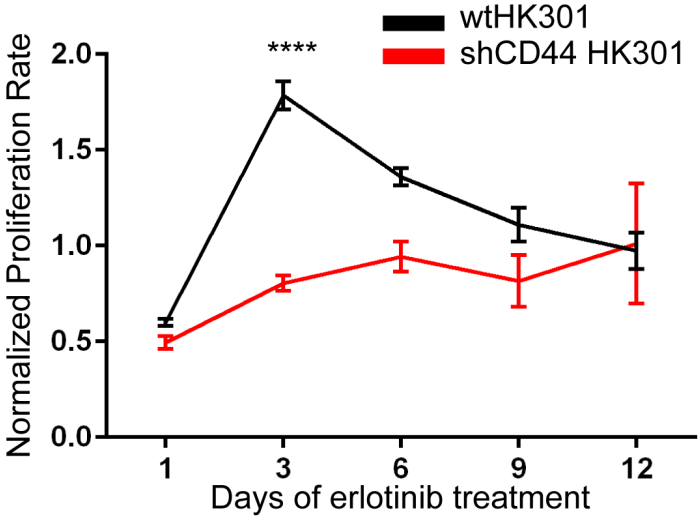
wtHK301
shCD44 HK301
Normalized Proliferation Rate
Days of erlotinib treatment

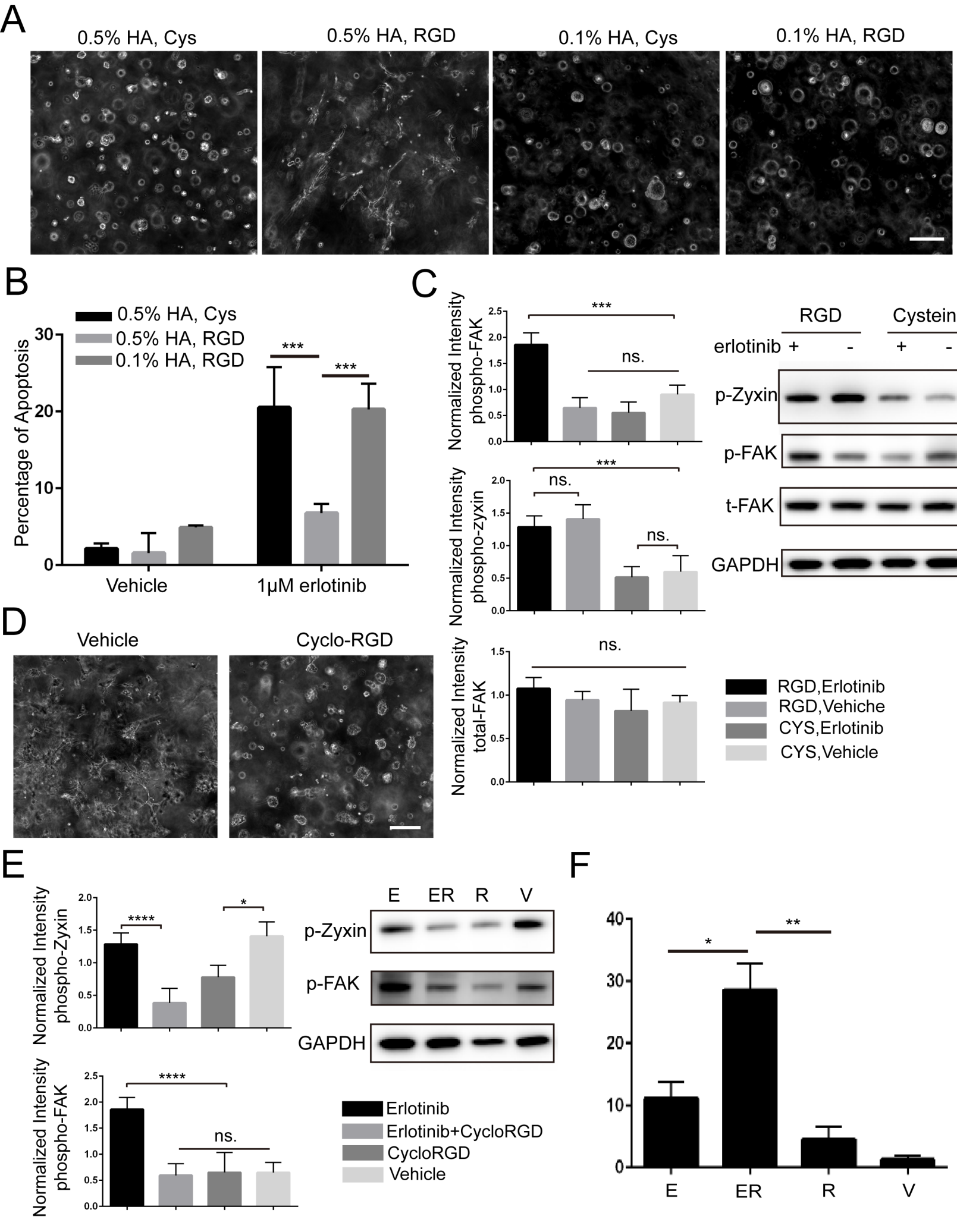
A
0.5% HA, Cys
0.5% HA, RGD
0.1% HA, Cys
0.1% HA, RGD
B
0.5% HA, Cys
0.5% HA, RGD
0.1% HA, RGD
Percentage of Apoptosis
***
***
Vehicle
1μM erlotinib
C
Normalized Intensity phospho-FAK
***
ns.
Normalized Intensity phospho-zyxin
***
ns.
ns.
Normalized Intensity total-FAK
ns.
RGD
Cysteine
erlotinib + - + -
p-Zyxin
p-FAK
t-FAK
GAPDH
RGD,Erlotinib
RGD,Vehiche
CYS,Erlotinib
CYS,Vehicle
D
Vehicle
Cyclo-RGD
E
Normalized Intensity phospho-Zyxin
****
*
Normalized Intensity phospho-FAK
****
ns.
E ER R V
p-Zyxin
p-FAK
GAPDH
Erlotinib
Erlotinib+CycloRGD
CycloRGD
Vehicle
F
*
**
E
ER
R
V